

Nanoscale

Accepted Manuscript



This is an *Accepted Manuscript*, which has been through the Royal Society of Chemistry peer review process and has been accepted for publication.

Accepted Manuscripts are published online shortly after acceptance, before technical editing, formatting and proof reading. Using this free service, authors can make their results available to the community, in citable form, before we publish the edited article. We will replace this *Accepted Manuscript* with the edited and formatted *Advance Article* as soon as it is available.

You can find more information about *Accepted Manuscripts* in the [Information for Authors](#).

Please note that technical editing may introduce minor changes to the text and/or graphics, which may alter content. The journal's standard [Terms & Conditions](#) and the [Ethical guidelines](#) still apply. In no event shall the Royal Society of Chemistry be held responsible for any errors or omissions in this *Accepted Manuscript* or any consequences arising from the use of any information it contains.

Cite this: DOI: 10.1039/c0xx00000x

www.rsc.org/xxxxxx

ARTICLE TYPE

Magnetic/NIR-thermally responsive hybrid nanogels for optical temperature sensing, tumor cell imaging and triggered drug release

Hui Wang, Jinhui Yi, Sumit Mukherjee, Probal Banerjee and Shuiqin Zhou*

Received (in XXX, XXX) Xth XXXXXXXXX 20XX, Accepted Xth XXXXXXXXX 20XX

DOI: 10.1039/b000000x

The paper demonstrates a class of multifunctional core-shell hybrid nanogels with fluorescent and magnetic properties, which have successfully been developed for simultaneous optical temperature sensing, tumor cell imaging and magnetic/NIR-thermally responsive drug carrier. The as-synthesized hybrid nanogels were designed by coating bifunctional nanoparticles (BFNPs, fluorescent carbon dots embedded in the porous carbon shell and superparamagnetic iron oxide nanocrystals clustered in the core) with a thermo-responsive poly(N-isopropylacrylamide-co-acrylamide) [poly(NIPAM-AAm)]-based hydrogel as shell. The BFNPs in hybrid nanogels not only demonstrate excellent photoluminescence (PL) and photostability due to the fluorescent carbon dots embedded in the porous carbon shell, but also has targeted drug accumulation potential and magnetic thermal conversion ability due to the superparamagnetic iron oxide nanocrystals clustered in the core. The thermo-responsive poly(NIPAM-AAm)-based gel shell cannot only modify the physicochemical environment of the BFNPs core to manipulate the fluorescence intensity for sensing the variation of the environmental temperature, but also regulate the release rate of the loaded anticancer drug (curcumin) by varying the local temperature of environmental media. In addition, the carbon layer of BFNPs can adsorb and convert the NIR light to heat, leading to a promoted drug release under an NIR irradiation and improving the therapeutic efficacy of drug-loaded hybrid nanogels. Furthermore, the superparamagnetic iron oxide nanocrystals in the core of BFNPs can trigger localized heating using an alternating magnetic field, leading to a phase change in the polymer gel to trigger the release of loaded drugs. Finally, the multifunctional hybrid nanogels can overcome cellular barriers to enter the intracellular region and light up the mouse melanoma B16F10 cells. The demonstrated hybrid nanogels would be an ideal system for the biomedical applications due to their excellent optical properties, magnetic properties, high drug loading capacity and responsive drug release behavior.

1. Introduction

With the development of nanomedicine, multifunctional hybrid nanogels have gained significant momentum among an increasing number of researchers because they demonstrate wide biomedical applications including drug carrier, sensor and bioimaging.¹⁻³ In particular, responsive hybrid nanogels as drug carrier have been the focus of experimental research due to their controlled drug release in response to external stimuli such as temperature, pH, light, bacteria and so on.⁴⁻¹¹ Although multifunctional hybrid nanogels have reduced the toxicity of many drugs by encapsulating drug into biocompatible polymer and improving the therapeutic efficacy of hybrid nanogels by controlling the drug release behavior, the main problem is still represented by the actual accumulation of drug-loaded hybrid nanogels at the tumor site. Two ways have been applied to enhance the accumulation of drug-loaded hybrid nanogels at the tumor site: passive accumulation and active retention mechanisms.^{12,13} In general, the passive accumulation of drug-loaded hybrid nanogels at the tumor site based on the permeation of hybrid nanogels through tumor vascular vessels will dramatically reduces due to the presence of blood flow together

with the dilution of the nanogels in the bloodstream during the circulation time.^{14,15} Active retention mechanisms that rely on the specific targeting of tumor tissues via molecular recognition units present at the carrier surface is an alternative technology to solve the aggregation of drug carrier at the tumor site.¹³ Despite their high efficiency for the target of drug carrier, the way has been found to be limited by complex synthesis process.

Recently, much research focus on the synthesis of magnetic-functional hybrid nanogels by loading superparamagnetic nanoparticles into stimuli-responsive polymers, which supplied a convenient tool for remotely enhancing drug accumulation in the tumor site.¹⁶⁻³³ Additionally, magnetic hybrid nanogels, exposed to appropriate alternating current (AC) magnetic field, not only generate heat for hyperthermia treatment to kill tumor cells in cancer therapy, but also provide the external heat to trigger the drug release from the temperature-responsive hybrid nanogels.²¹⁻³⁰ Up to now, although great progress on the development and application of magnetothermally-responsive hybrid nanogels have been obtained, multifunctional hybrid nanogels as in vivo drug delivery carriers are still limited due to the inter-particle aggregation and weak control of superparamagnetic nanoparticles occurred when the polymer transfer from a coil to a shrunk state

under an external stimulus. Near-infrared (NIR) light, an alternative external stimulus, have widely been used to control the drug release due to their low energy absorption, deep penetration and minimum side effects for human tissue and organs.^{34,35} In addition, NIR-triggered nanocarrier brings a new opportunity to release the loaded drug at a desired time and in a desired area by applying a NIR light on the tumor site.³⁶⁻⁴⁰ By introducing bifunctional nanoparticles (BFNPs) with fluorescent and magnetic properties into the thermally-responsive polymer gel, the formed multifunctional hybrid nanogels can not only demonstrate excellent optical properties for bioimaging and biosensor, but also be used as highly efficiently carrier for magnetic/NIR-controlled drug release. Liz-Marzán et al. reported the synthesis of multifunctional composite microgels via in situ Ni growth on pNIPAM-coated Au nanoparticles. The novel colloidal composites realized the combination of multiple functionalities including optical detection, magnetic manipulation, molecular trapping, and thermal response.⁴¹ However, the noble metal core in multifunctional hybrid nanogels have disadvantages with high cost and potential cytotoxicity.⁴²⁻⁴⁶ In addition, the magnetic component composed of Ni is not suitable for magnetothermally-responsive drug carrier because of its potential cytotoxicity, inter-particle aggregation and poor biocompatibility in vivo.^{47,48} Furthermore, the responsive drug release behavior of the as-synthesized multifunctional composite microgels as nanocarrier has not been explored as far as we know. The purpose of this manuscript is to synthesize a class of multifunctional hybrid nanogels based on biocompatible BFNPs with fluorescent and superparamagnetic properties,⁴⁹⁻⁵⁰ and discuss their potential applications as sensor, imaging agent and responsive drug carrier.

In this manuscript, we have successfully designed a class of multifunctional core-shell hybrid nanogels based on previously reported biocompatible BFNPs with a core-shell structure (fluorescent carbon dots embedded in the porous carbon shell and magnetic iron oxide nanocrystals clustered in the core⁵¹) for simultaneous optical temperature sensing, tumor cell imaging and magnetic/NIR-responsive drug carrier. As illustrated in Fig. 1, the spherical hybrid nanogel loaded with drug molecules of curcumin is comprised of BFNP as core, thermo-responsive poly(NIPAM-AAm)-based gel as shell. The carbon layer in BFNPs not only provide fluorescent carbon dots for optical sensing, cellular imaging and photothermal ability for NIR-responsive drug release, but also enhance the drug loading capacity based on the hydrophobic associations between the conjugated carbon and the curcumin molecules compared with the reported carbon-based responsive nanogels.⁵² Meanwhile, the magnetic core composed of superparamagnetic nanocrystals cluster in BFNPs is expected to provide stable magnetic separation, targeted drug accumulation and magnetic-thermal ability for magnetic-responsive drug release. Furthermore, the thermal-responsive poly(NIPAM-AAm)-based gel shell is designed to serve as intelligent drug carriers with high drug loading capacity. The reversible swelling and shrinking of the poly(NIPAM-AAm) shell in response to temperature change will not only modify the physicochemical environment of the embedded BFNP to manipulate the optical properties of core for sensing on local environment, but also change the mesh size of the gel networks to regulate the drug release. The curcumin molecules in the thermo-responsive hybrid nanogels may also kill tumor cell and provide basal chemotherapy for daily care under the exogenous activation strategy. Such a hybrid nanogel provides a multifunctional

nanoplatfor for biomedical applications as sensors, imaging agent and responsive drug carrier.

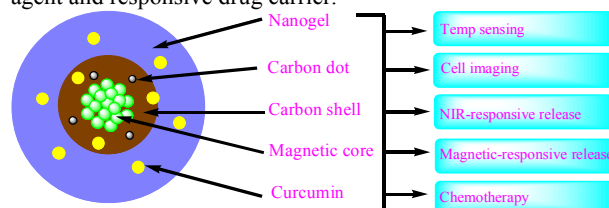


Fig. 1. Schematic illustration of multifunctional core-shell hybrid nanogels. The anticancer drug (curcumin) and BFNP are coated by an outer poly(NIPAM-AAm)-based gel layer to offer both stability in aqueous media and temperature sensitivity.

2. Materials and methods

2.1 Materials

All chemicals were purchased from Aldrich. NIPAM was recrystallized from a 1:1 hexane-acetone mixture and dried in vacuum. Curcumin was purified with anhydrous ethanol. Ferrocene ($\text{Fe}(\text{C}_5\text{H}_5)_2$, $\geq 98\%$), hydrogen peroxide (H_2O_2 , 30%), acetone ($\text{C}_3\text{H}_6\text{O}$) and ethanol ($\text{C}_2\text{H}_6\text{O}$). Ammonium persulfate (APS), sodium dodecyl sulfate (SDS), N,N-methylenebisacrylamide (BIS) and acrylamide (AAm) were used as received without further purification. The water used in all experiments was of Millipore Milli-Q grade.

2.2. Synthesis of fluorescent carbon shell and magnetic core nanoparticles

BFNPs with fluorescent and magnetic properties were synthesized via a reported one-step process.⁵¹ Ferrocene (0.10 g) were dissolved in acetone (30 mL). After intense sonication for 30 min, 2.5 mL of hydrogen peroxide (30% in water) was slowly added into the above mixture solution, which then was vigorously stirred for 30 mins. After that, the precursor solution was transferred to the Teflon-lined stainless autoclave with the total volume of 50.0 mL, and then heated to and maintained at 200 °C. After 48 h, the autoclave was cooled naturally to room temperature. The products from the Teflon-lined stainless autoclave were magnetized for 10 min by a magnet with 0.20 T, and the supernatant was discarded. The precipitates were then washed with acetone three times to remove excess ferrocene. Finally, the black products were dried at room temperature in a vacuum oven.

2.3. Synthesis of multifunctional core-shell hybrid nanogels

Multifunctional core-shell hybrid nanogels were prepared by free radical precipitation copolymerization of NIPAM, AAm and BFNPs using APS as an initiator. In a 250 mL round-bottom flask equipped with a stirrer, a N_2 gas inlet, and a condenser, the as-prepared BFNPs suspension (47.5 mL, 0.1 g/L) was heated to 30 °C, followed by addition of NIPAM (0.7024 g), AAm (0.0509 g), BIS (0.0368 g) and SDS (0.0254 g) under stirring. After the temperature was raised to 70 °C and keep 60 min under N_2 atmosphere, the polymerization was initiated by adding 2.50 mL APS with the concentration of 2 mM. The polymerization was allowed to proceed for 4 h. The solution was centrifuged three times at 20,000 rpm (30 min, Thermo Electron Co. SORVALL[®] RC-6 PLUS superspeed centrifuge) with the supernatant discarded and the precipitate redispersed in 50 mL deionized water. The resultant hybrid nanogels with a volume of 50 mL were further purified by 7 days of dialysis (Spectra/Por molecularporous membrane tubing, cutoff 12000-14000) against very frequently changed water at room temperature (~ 22 °C).

2.4. Preparation of curcumin-loaded hybrid nanogel

Curcumin, a kind of anti-cancer drug, was loaded into the hybrid nanogels by complexation method. The hybrid nanogel dispersion (5 mL, pH=4.0) was placed in a vial and stirred for 30

min in a water bath (20 °C). Then, 4 mL fresh curcumin solution of 1 mg/mL in anhydrous ethanol was added dropwisely into hybrid nanogel. The immediate slight cloudy revealed the complexation of the curcumin molecules with the polymer chains in hybrid nanogels. After stirring for 12 h under a dark light, the suspension was centrifuged at 5000 rpm for 30 min at 20 °C. In order to remove unloaded curcumin, the precipitate was redispersed in 5 mL HCl solution of pH=4.0, and further purified by repeated centrifugation and washing until the separated solution is clear. All the washed and separated solutions were collected and combined. The concentration of free curcumin in the combined solution was determined by UV-vis spectrometry at 435 nm. The loading efficiency was calculated by Equations (1):

$$(1) \text{ Loading efficiency } \% = \frac{M_0 - M_t}{M_0} \times 100\%$$

are the quantity of curcumin in the initial solution and separated solution, respectively. The influence of loading time and temperature on loading efficiency of multifunctional hybrid nanogels were discussed in the preparation process of curcumin-loaded hybrid nanogel. In addition, curcumin was also loaded into the poly(NIPAM-AAm) nanogels and BFNPs under the same experiments conditions.

2.5. Curcumin release of the curcumin-loaded hybrid nanogel

The in vitro release test of curcumin from the hybrid nanogels was evaluated by the dialysis method. The separated curcumin-loaded hybrid nanogels was redispersed in 10 mL HCl solution of pH=4.0. A dialysis bag filled with 1 mL diluted curcumin-loaded hybrid nanogels was immersed in 50 mL 0.005 M buffer solutions of pH = 6.15 but at different temperatures including 41 °C, 39 °C, 37 °C, 22 °C. The NIR-responsive release experiments of curcumin-loaded hybrid nanogels at physiological temperature of 37 °C were performed with 5 min NIR (1.5 W/cm²) irradiation at a certain time interval. The magnetic-responsive release experiments of curcumin-loaded hybrid nanogels at physiological temperature of 37 °C were performed with 30 min alternating magnetic field induced using magnetic generator (100 V, 0.8A, 50 Hz) at a certain time interval. The released curcumin outside of the dialysis bag was sampled at defined time period and assayed by UV-vis spectrometry at 430 nm. Cumulative release is expressed as the total percentage of drug released through the dialysis membrane over time.

2.6. Internalization of multifunctional hybrid nanogels into mouse melanoma cells B16F10

Round glass cover slips were placed in wells of a 24-well plate and treated with 0.1% poly-L-lysine in 100 mM phosphate buffered saline (PBS) solution for 40 min. Following the treatment, the solution was aspirated and the wells were washed with PBS 3 times each. Next, B16F10 cells (2×10⁴ cell/well) were plated on the glass coverslips at 80% confluence in DMEM containing 10% FBS and 1% penicillin-streptomycin. After 24 h, 500 µL of multifunctional hybrid nanogel (50 mg/mL) in serum-free DMEM were respectively added to the marked wells. In a control well, 500 µL of serum-free DMEM was added. The plate was incubated at 37 °C for 2 h. The medium was then aspirated and fresh serum-free DMEM was added to each well. Finally, the coverslips with cells were removed from the wells and mounted onto slides for confocal microscopy study.

2.7. In vitro cytotoxicity of hybrid nanogels and curcumin-loaded hybrid nanogels with or without NIR irradiation

In this study, B16F10 cells were cultured in the 96 wells microplate in 100 µL medium containing about 2,000 cells seeded into each wells. After an overnight incubation for attaching, the medium was removed and another 100 µL medium containing hybrid nanogels or curcumin-loaded hybrid nanogels was added to make the final extract concentration of 200 µg/mL,

150 µg/mL, 100 µg/mL and 50 µg/mL, respectively. Wells used the normal medium without drugs were used as control. For photothermal treatments, the cells were irradiated with 1.5 W/cm² NIR light for 5 min. After incubated for 24 h, 10 µL of 3-(4,5-dimethyl-2-thiazolyl)-2,5-diphenyltetrazolium bromide (MTT) solution (5 mg/ml in PBS) is added into the wells. The wells were further incubated in a humidified environment of 5 % CO₂ and 37 °C for 2 h. The medium were removed after 2 h and 100 µL of DMSO solution is added. The plates were gently agitated until the formazan precipitate was dissolved, followed by measurement of OD value by spectrophotometer at 570 nm and 690 nm.

2.8. Characterization

The UV-vis absorption spectra were obtained on a Thermo Electron Co. Helios β UV-vis Spectrometer. The powder X-ray diffraction (XRD) patterns were collected on a Japan Rigaku D/MAX-γA X-ray diffractometer equipped with Cu Kα radiation (λ = 1.542 Å) over the 2θ range of 10–70°. The PL spectra were respectively obtained on a JOBIN YVON Co. FluoroMax[®]-3 Spectrofluorometer equipped with a Hamamatsu R928P photomultiplier tube, calibrated photodiode for excitation reference correction from 200 to 980 nm, and an integration time of 1 s. The transmission electron microscopy (TEM) images were taken on a FEI TECNAI transmission electron microscope at an accelerating voltage of 100 kV. High-resolution TEM images were characterized by a JEM 2100 instrument with an acceleration voltage of 200 kV. Energy-dispersive X-ray analysis was obtained with an EDAX detector installed on the JEM 2100. The photothermal experiments on the hybrid nanogels were conducted using a Philips infrared reflector lamp with a power density of 1.5 W cm⁻² and a filter to block ultraviolet-visible light. The B16F10 cells incorporated with hybrid NPs were imaged using a confocal laser scanning microscopy (LEICA TCS SP2 AOBST[™]) equipped with a HC PL APO CS 20×0.7 DRY lens. A UV (405 nm) light was used as the light source. Dynamic light scattering (DLS) was performed on a standard laser light scattering spectrometer (BI-200SM) equipped with a BI-9000 AT digital time correlator (Brookhaven Instruments, Inc.) to measure the hydrodynamic radius (R_h) distributions. A He-Ne laser (35 mW, 633 nm) was used as the light source. The hybrid nanogels dispersion was passed through Millipore Millex-HV filters with a pore size of 0.45 µm to remove dust before the DLS measurement. A superconducting quantum interference device magnetometer (Quantum Design MPMS XL-7) was used to measure the magnetic properties of as-prepared samples.

3. Results and Discussion

3.1. Synthesis, structure and properties of BFNPs-functionalized hybrid nanogels

The procedure to prepare the multifunctional core-shell hybrid nanogels involves the first synthesis of BFNPs as core, followed by precipitation copolymerization of the NIPAM and AA comonomers that are complexed with carbon layer on the surface of BFNPs. Fig. 2a shows the typical TEM image of the obtained BFNPs, which shows a clear core-shell structure and a spherical morphology with an average size of ~95 nm in diameter. The XRD pattern of the obtained BFNPs (See Supplementary Information Fig. S1) with reflections indexed as 220, 311, 400, 422, 511, 440 confirms the presence of magnetic Fe₃O₄ nanocrystals with a size about 9.2 nm calculated from the Debye-Scherrer formula.⁵³ The typical SAED pattern of a single BFPN (Fig. S2b) with the clear sharp diffraction rings further indicates the polycrystalline nature of the BFNPs. Its arcs and rings could be indexed as (220), (311), and (222) reflections from the magnetite. The HRTEM image of a section from the single BFPN

(Fig. S2a) further manifests the core-shell nanostructure with dark-contrasted iron oxide nanocrystals in the core and light-contrasted carbon layer as the shell. Meanwhile, as shown in Fig. S2c, some nanocrystals with a size about 4 nm can be easily found in the carbon shell. The 2D lattice fringes of these nanocrystals demonstrate an inter-planar distance about 0.311 nm, which corresponds to the (002) lattice planes of graphitic (sp^2) carbon.⁵⁴ The energy dispersive spectrum (Fig. S2d) from the single nanocrystal embedded in the shell only reveals the presence of C and Cu elements, which further support that these nanocrystals are carbon dots (Cu is from the copper grid for TEM sample preparation). The emitted blue light can be obviously found after the aqueous dispersion of BFNPs was exposed under UV light (365 nm), indicating its excellent fluorescent property. A dynamic light scattering (DLS) was used to further characterize the stability and size of BFNPs, which are shown in Fig. S3. The narrow size distribution with an overall hydrodynamic diameter of 106 nm in distilled water shows that the BFNPs are stable in distilled water and do not form aggregates. As expected, the increases (from 95 nm to 106 nm) in the hydrodynamic diameter of BFNPs by 11 nm were observed because of the existence of hydrophilic carboxyl group.⁵¹ These hydrophilic $-COOH$ and/or $-OH$ groups on the BFNPs not only enable the nanoparticles to be dispersed very well in water, but also can form hydrogen bonds with the amide groups in the AAm monomers, thus forming BFNPs-AAm complexes in water. After the copolymerization and crosslinking of these BFNPs-complexed AAm monomers with the NIPAM monomers, it is expected that the BFNPs will be immobilized into the resultant thermo-responsive poly(NIPAM-AAm) nanogel network. Fig. 2b shows a typical TEM image of the resultant poly(NIPAM-AAm)-BFNPs hybrid nanogel particles in dried state. After the surface coating of BFNPs with a thermo-responsive poly(NIPAM-AAm)-based hydrogel, the change in size due to the polymer growth is also confirmed by TEM. The dried hybrid nanogels have a spherical shape with an average diameter about 170 nm. Multifunctional hybrid nanogels are well dispersed on the TEM grid giving a clear indication of the growth of the polymer gel shell around each individual starting bead. In addition, TEM image (Fig. 1b) has clearly demonstrated their core-shell structure with a polymer shell thickness of 35 nm. These results show that the BFNPs are successfully encapsulated in the poly(NIPAM-AAm) nanogel.

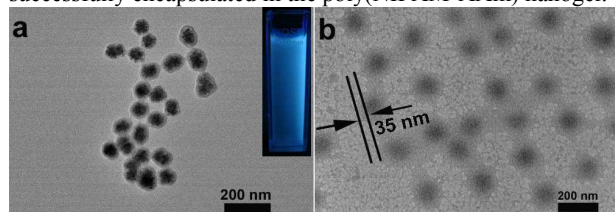


Fig. 2. (a) TEM images of the as-obtained BFNPs, (b) TEM image of the as-obtained hybrid nanogels.

3.2. Temperature-induced volume phase transition of the hybrid nanogels

Fig. 3a shows the temperature-induced volume phase transitions of the multifunctional hybrid nanogels dispersed in PBS of pH = 7.40, in terms of the change of D_h measured at a scattering angle of $\theta = 60^\circ$. It is very clear that the temperature of dispersion medium can significantly influence the size of the hybrid nanogels due to the existence of thermo-responsive poly(NIPAM-AAm)-based gel shell. The DLS diameter of the hybrid nanogels changes substantially from 336 nm at 16 °C to 186 nm at 50 °C, due to the phase transition from the random coil to the collapse state of the crosslinked P(NIPAM-AAm) chains when the temperature was increased above 36 °C. In addition,

compared with the size (106 nm) of BFNPs in Fig. S3, the size of hybrid nanogels at 24 °C is about 320 nm. This size is obviously larger than the size of BFNPs, which indicates that the thermo-responsive poly(NIPAM-AAm)-based gel shell have been coated on the surface of BFNPs. The size distributions of the hybrid nanogels at different temperatures (16 °C, 36 °C and 50 °C) are shown in Fig. 3b. These hybrid nanogels are nearly monodisperse regardless of their swelling/shrinking states. It is important to point out that in our multifunctional core-shell hybrid nanogels embedded with superparamagnetic iron oxide nanocrystals cluster, the polymer contraction involves a change of the volume at individual hybrid nanogel and it does not involve inter-particle agglomeration. The prohibited inter-particle agglomeration of the hybrid nanogels should be attributed to both the hydrophilic $-COOH$ and/or $-OH$ groups on the carbon layer of BFNPs and the hydrophilic polyAAm segments copolymerized in the polymer gel shell. This behavior is obviously different from that of individual PNIPAM-coated iron oxide nanocrystals in which the thermo-responsive behavior drives the inter-particle aggregation, leading to micrometre aggregates. The thermo-responsive behavior of our multifunctional hybrid nanogels is definitely more advantageous when the hybrid nanogels are designed for drug delivery as in vivo aggregation should be avoided.

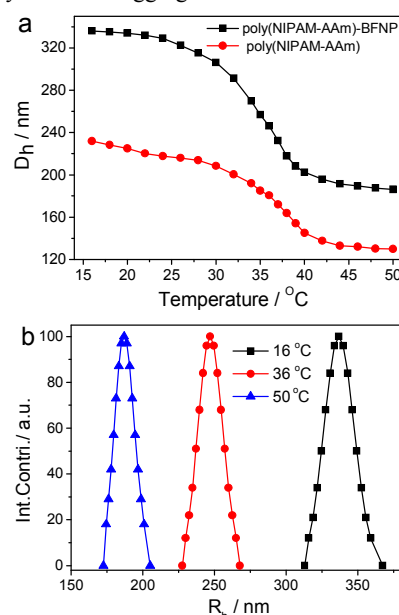


Fig. 3. (a) Temperature dependence of the average D_h values of poly(NIPAM-AAm) nanogels and poly(NIPAM-AAm)-BFNP hybrid nanogels in PBS of pH = 7.40 at a scattering angle $\theta = 60^\circ$. (b) Size distributions of the hybrid nanogels at different temperatures (16 °C, 36 °C and 50 °C).

3.3. Temperature-sensitive PL property of the hybrid nanogels

Fig. 4a shows typical UV-visible absorption spectra of the BFNPs, poly(NIPAM-AAm) nanogels and poly(NIPAM-AAm)-BFNP hybrid nanogels, respectively. The encapsulation of BFNPs within the poly(NIPAM-AAm) shell has been also confirmed by their UV-visible absorption spectra. While the poly(NIPAM-AAm) nanogel has no significant absorption at wavelength above 264 nm, there is a clear broad peak centered at 264 nm in the curve of BFNPs, which represent the typical absorption of an aromatic π system and is similar to that of polycyclic aromatic hydrocarbons.^{55,56} Meanwhile, the hybrid nanogels have a similar absorption peak (264 nm), which indicates that the BFNPs have been coated by thermo-responsive poly(NIPAM-AAm)-based hydrogels. Fig. 4b shows the PL

spectra of multifunctional hybrid nanogels with the excitation wavelength of 264 nm according to its UV-vis absorption spectra. An emission peak at 377 nm is found. The PL excitation spectrum of the hybrid nanogels recorded at 377 nm (Fig. S4a) shows a peak at ~ 340 nm. By selecting 340 nm as excitation wavelength, we obtained a PL spectrum with a maximal emission intensity at about 430 nm (Fig. S4b). In addition, the PL spectra obtained using different excitation wavelengths (Fig. S4b) show that the hybrid nanogels demonstrate excitation-dependent emission property. Although the luminescence mechanism of CDs is still controversial, it has been widely accepted that the luminescence of CDs involve the surface traps in the radiative transition of CDs.⁵⁷⁻⁶⁰ In our BFNPs, the CDs are embedded in the porous carbon with various surface functional groups including C=O, -OH, and O=C-OH.⁵¹ In addition, small molecular monomers can easily diffuse into the surface area of the CDs through the porous carbon. After polymerization of the monomers, the poly(NIPAM-AAM) gel with amide groups can also have direct contact with the CDs. These different surface groups of CDs embedded in the hybrid nanogels can introduce trapping states with different energy levels, leading the CDs to emit light varying with the excitation energy. The typical average luminescent lifetime of CDs ranges from 5.21 ns to 7.31 ns, depending on the surface property of CDs.⁶⁰⁻⁶¹ Meanwhile, the temperature dependent PL spectra of the poly(NIPAM-AAM)-BFNPs hybrid nanogels have also been found. It is very clear that the shrinking of hydrogel shell induced by increasing the temperature could significantly enhance the PL intensity of BFNPs emissions in the hybrid nanogels. In order to describe the relationship between the temperature induced volume phase transitions and PL intensity enhancement of the multifunctional hybrid nanogels, the PL intensity at 377 nm under the different measurement temperatures was plotted, as shown in Fig. 4c. The comparison of Fig. 4c with Fig. 3a indicates that a conspicuous increase in fluorescence intensity occurred at nearly the same temperature when the nanogel shell began to shrink. More importantly, a linear correlation between the PL intensity and temperature can be established across the temperature range of 20-42 °C (inset of Fig. 4c), which is essential for the hybrid nanogels to serve as optical temperature sensor.

The enhancement of the PL intensity of multifunctional hybrid nanogels should be attribute to two factors. One is the refractive index increase of the gel shell due to the shrinkage of polymer networks, which leads to an enhancement in the Rayleigh scattering due to a larger refractive index contrast of the condensed polymer networks with the solvent.⁶² The other one might be from the different nonradiative energy loss paths, which is related to the reduction of the number of surface defects. According to the previous reports, the nonradiative energy loss paths are highly dependent on the environmental nature surrounding the carbon dots.⁶³ This phenomenon of BFNPs with the fluorescent carbon dots embedded in the porous carbon shell is similar to the temperature-induced PL quenching of colloidal quantum dots (QDs) dispersed in water, where the freezing of dispersion medium propagates the strain to the surface of the QDs, leading to surface quenching states.⁶⁴ Therefore, when the temperature increases, the hybrid nanogels will be in shrunk states, which decreases the elastic tension and consequently reduce the number of surface trap states acting as emission quenching centers, thus the PL intensity increases. While we speculate the possible reasons to explain the temperature-induced PL enhancement of the shrunk hybrid nanogels, we do observe the direct evidence on the PL enhancement of the hybrid nanogels upon the temperature increase. Simply dispersed in water and irradiated with a 365 nm UV-lamp, the hybrid nanogel

dispersions exhibit different color at 15.5 °C and 50.0 °C, which is observable by naked eye (photographs in Fig. S5). Fig. 4d shows the PL intensity change of multifunctional hybrid nanogels experiencing ten cycles of heating and cooling adjustment. The PL spectra were fully reproducible after the repeated heating and cooling due to the reversible thermo-responsive volume phase transition of the poly(NIPAM-AAM)-based gel shell. The reversible optical property change is critical for the hybrid nanogels to sense the local environmental change. As shown in Fig. S6, negligible changes of the fluorescence response can be obtained upon 2 h continuous exposure to the excitation light using a fluorescence spectrophotometer at 50.0 °C. The results indicate that the multifunctional hybrid nanogels have an excellent photostability against light illumination.

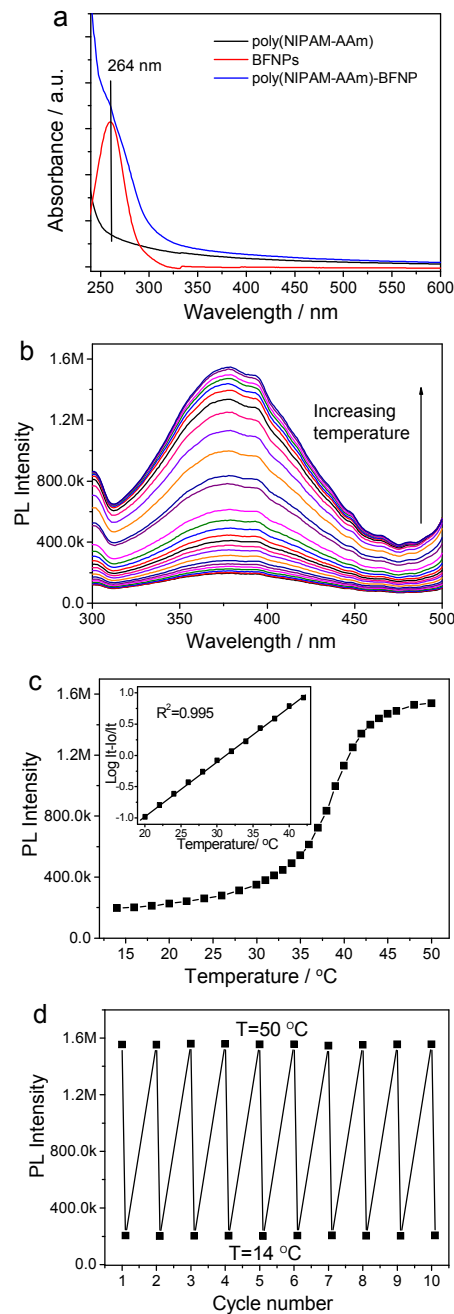


Fig. 4. (a) Typical UV-Vis absorption spectra of BFNPs, poly(NIPAM-AAM) nanogels and poly(NIPAM-AAM)-BFNP hybrid nanogels. (b) Typical PL profiles of the hybrid nanogels

under the different temperature, taken at 2.0 °C intervals from bottom to top. (c) The effect of temperature on the PL intensity of the hybrid nanogels. (d) Reversible PL intensity change of the hybrid nanogels after ten cycles of repeated heating (50.0 °C) and cooling (14.0 °C). All measurements were made in PBS of pH = 7.4. Excitation wavelength = 264 nm.

3.4. Drug loading and NIR-responsive drug release of the hybrid nanogels

The thermo-responsive change in volume of the polymer shell can be exploited for both the loading and the release of drug molecules. Curcumin, a yellow natural compound, was selected as a representative drug for investigating the loading and release of the hybrid nanogels because of their excellent properties including antioxidant, antibacterial, antifungal, antiviral, anti-inflammatory, antiproliferative, and pro-apoptotic effects.^{65,66} The loading experiment shows that the curcumin molecules can be readily loaded into the multifunctional hybrid nanogels by simply mixing the curcumin into the PBS solution of hybrid nanogels. The drug loading content reaches 65.5 mg/g (number of mg drug in 1 g of dried carrier), which means that the hybrid nanogels will be promising drug carriers. A UV-Vis absorption peak at around 430 nm (the characteristic absorption wavelength of curcumin) in Fig. S7 confirms the formation of drug-loaded hybrid nanogels. Meanwhile, the quantitative analysis shows that the curcumin loading content of the free poly(NIPAM-AAm) nanogels and BFNPs are 32 mg/g and 37.2 mg/g, respectively, which confirms that the hybrid nanogels have a higher loading capacity for hydrophobic curcumin drug than the free polymer nanogels and BFNPs. This increased curcumin loading capacity of the hybrid nanogels might be attributed to the conjugated aromatic carbon structures of the BFNPs embedded in the gel network, which can associate with curcumin molecules more strongly. In addition, by comparing the photographs in Fig. S8, it can be found that the aqueous dispersion of the curcumin-loaded hybrid nanogels is a homogeneously dispersed formulation with its hue derived from the natural color of curcumin, which indicates that the as-synthesized multifunctional hybrid nanogels can be used as carrier of hydrophobic drug.⁶⁷

Having demonstrated the curcumin loading ability of the hybrid nanogels, the release behavior of curcumin from the multifunctional hybrid nanogels was studied at different temperature in a PBS buffer solution at pH 7.4. Fig. 5a shows the release kinetics of curcumin from the hybrid nanogels under different temperatures. The release kinetics of curcumin from the hybrid nanogels is temperature dependent. The increase in temperature could significantly enhance the release rate of curcumin from the hybrid nanogels. When the temperature of releasing medium is at 22 °C (below the LCST), only 20.9 % curcumin was released from hybrid nanogels after 60 h. On the other hand, at temperature above the LCST, the poly(NIPAM-AAm) shell becomes hydrophobic and collapses rapidly, which cannot only squeeze out the drug molecules quickly from the polymer shell, but also reduce the diffusion path length of drug molecules. Therefore, the amount of the released curcumin from the hybrid nanogels reached 35.3%, 47.4%, and 70.4% at a temperature of 37 °C, 39 °C, and 41 °C, respectively, after the same time period of 60 h. The observed temperature dependency of curcumin release should be associated with the outer thermo-sensitive poly(NIPAM-AAm)-based gel layer. As shown in Fig. 3, the increase in temperature can induce a gradual shrinkage of nanogels, leading to a thinner thickness and a smaller mesh size of the outer poly(NIPAM-AAm)-based gel layer. Therefore, the multifunctional hybrid nanogels can be used as external stimuli-

responsive nanocarrier to trigger the drug release from the interior of hybrid nanogel to the external medium.

In addition to the endogenous activation strategy to regulate the curcumin release via the temperature variation in the pathological microenvironment, a highly orthogonal external NIR irradiation can provide an external triggered release of the loaded drug due to the photothermal conversion ability of fluorescent carbon dots in the BFNPs. It should be mentioned that the maximal UV/vis absorption peak of BFNPs is around 264 nm. However, it is known that the highly energetic UV light can cause damage to the biological tissues and thus is not suitable for therapeutic purpose. In contrast, NIR light with low energy absorption and deep penetration for biological tissues is much less harmful. Thus, NIR light is more preferable to be used for photothermal therapy or light-responsive drug delivery to improve the therapeutic efficacy while minimizing side effects. It has been reported that graphene nanoparticles (~10-20 nm) can be used for efficient NIR-light photothermal therapy.^{68,69} The mechanism of such a photothermal conversion of the graphene nanoparticles is their high absorbance in NIR range benefited from the aromatic, highly π -conjugated carbon structure. Our BFNPs with the aromatic π -conjugated carbon dots embedded in the carbon layer also demonstrate significant absorption in the NIR light range (Fig. S9a). Thus, the hybrid nanogels prepared from the BFNPs have high photothermal conversion ability (Fig. S9b). Fig. 5b shows the release kinetics of curcumin from the hybrid nanogels immersed in a buffer solution of pH = 7.4 at 37 °C and irradiated by 1.5 W/cm² NIR light for 5 min at 0, 5, 60, and 92 h, respectively. An initial exposure (0 h) to the NIR light led to a burst release of drug. When the NIR light was turned off, heating immediately ceased and the drop in temperature brought the drug release back to its regular slow rates. The reason of NIR-accelerated curcumin release from the hybrid nanogels should involve both the temperature-induced shrinking of the poly(NIPAM-AAm)-based gel layer, producing a decreased diffusion path length for curcumin, and the increased mobility of curcumin molecules due to the brown motion at the elevated temperatures.

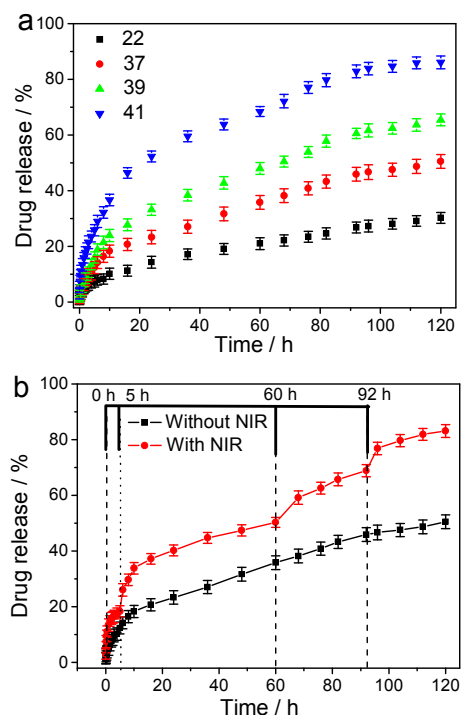


Fig. 5. (a) Releasing profiles of curcumin-loaded hybrid nanogels at different temperatures ($^{\circ}\text{C}$). (b) Releasing profiles of curcumin loaded hybrid nanogels at a constant temperature of 37°C , irradiated with/without 1.5 W/cm^2 NIR for 5 min at cumulative time of 0, 5, 60, and 92 h, respectively.

3.5. Magnetic property and magnetic-responsive drug release of the hybrid nanogels

The magnetic property of multifunctional core-shell hybrid nanogels was measured at 300 K in an applied magnetic field of up to 40000 Oe, as shown in Fig. 6a. The saturation magnetization (M_s) of the hybrid nanogels is 5.34 emu/g . The value of M_s is obviously lower than that of template BFNPs. This result could be attributed to two possible reasons. One is that the hybrid nanogels contain only about 40% of magnetic BFNPs, which reduces the relative mass ratio of the magnetic component and thus decrease the value of M_s per gram of hybrid nanogels. Another is that the polymer coating may adversely affect the magnetic property. The carbon layer is porous in BFNPs and thus monomers can easily diffuse into the surface area of the magnetic core. After polymerization, the polymer gel can have direct contact with the magnetic core, which could change the anisotropy and coordination for the surface magnetic atoms or even exchange electrons with the surface magnetic atoms. These surface property changes are known to influence the magnetic properties. In addition, no hysteric behaviour can be observed in Fig. 6a, indicating a superparamagnetic nature of these hybrid nanogels. When the solution of multifunctional hybrid nanogels is subjected to a magnetic field (0.30 T), the samples can be attracted toward the magnet side within half hour, as shown in inset of Fig. 6a. Slight agitation will bring the hybrid nanogels back into the original solution after the magnetic field was removed. The magnetic responsiveness and redispersibility of the newly designed hybrid nanogels is undoubtedly very important for future applications in bioseparation, storage, and magnetic targeting of the drug carriers to the pathological zones.

The suitability of the multifunctional hybrid nanogels as magnetic-responsive nanocarrier was examined due to the existence of superparamagnetic iron oxide nanocrystals cluster in the core of BFNPs. For this purpose, a certain amount of curcumin-loaded hybrid nanogels was placed in a magnetic generator producing an alternating magnetic field inside a thermostatic chamber at 37°C . Measurements of the total amount of curcumin accumulated in the supernatant were acquired at both the starting point of applying magnetic field and the time point after 30 min exposure to the magnetic field. Fig. 6b shows the release kinetics of curcumin from the hybrid nanogels immersed in a buffer solution of $\text{pH} = 7.4$ at 37°C and irradiated by an alternating magnetic field at 0.5, 5, 60, and 92 h, respectively. The release rate of curcumin loaded in hybrid nanogels shows an obvious enhancement when an alternating magnetic field was applied. When an alternating magnetic field was turned off, the drug release returns back to its regular rates similar to the release curve of hybrid nanogels at 37°C . Such an obvious release improvement in hybrid nanogels should be attributed to the intensive local heat produced by the magnetic-thermal conversion (Fig. S10) of the BFNPs under the alternating magnetic field. It should be mentioned that the drug release pattern shown in Fig. 6b is very similar to that shown in Fig. 5b, because we applied the external stimuli of alternating magnetic field at the same releasing stages of 0, 5, 60, and 92 h as those used for NIR irradiation stimuli. Both the NIR light irradiation and alternating magnetic field treatments produce local heat. The local heat will decrease the diffusion path length of curcumin due to the shrink of the poly(NIPAM-AAm)-based gel layer and increase the

65 brown motion of curcumin molecules due to the enhancement of local temperatures. This responsive release behavior reveals that the multifunctional hybrid nanogels have a potential for on-demand drug delivery system.

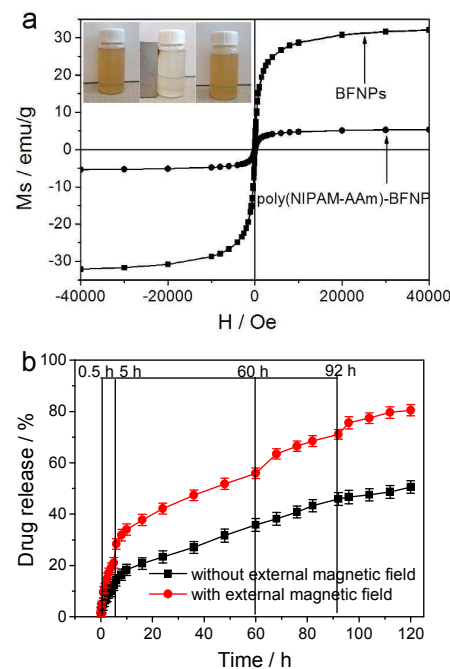


Fig. 6. (a) The hysteresis loop measured at room temperature for multifunctional core-shell hybrid nanogels. The inset is photographs of an aqueous hybrid nanogels dispersion in a vial (left) without magnetic field, (middle) with magnetic field, and (right) after the magnetic field is removed. (b) Releasing profiles of curcumin loaded hybrid nanogels at a constant temperature of 37°C , induced with/without an external magnetic field for 30 min at cumulative time of 0.5, 5, 60, and 92 h, respectively.

3.6. Tumor cell internalization of the hybrid nanogels

After confirming their responsive drug release behavior, mouse melanoma cells B16F10 were incubated with multifunctional hybrid nanogels to evaluate their cellular imaging function. As shown Fig. 7, the confocal microscopy images confirm that multifunctional hybrid nanogels can overcome cellular barriers to enter the intracellular region and light up the mouse melanoma B16F10 cells. Meanwhile, in order to further study the photostability of hybrid nanogels, laser scanning confocal images of mouse melanoma cells B16F10 incubated with the hybrid nanogels under different excitation time are demonstrated for long-term cellular imaging. Under irradiation of the laser with a wavelength of 405 nm, the BFNPs encapsulated in the poly(NIPAM-AAm)-based gels shell produced a bright fluorescence, which retained nearly the same PL intensity even after 30 min irradiation. No significant autofluorescence was observed under similar conditions. These results suggest the multifunctional hybrid nanogels have good photostability and are superior for fluorescent bioimaging. In addition, the top-to-bottom Z-scanning confocal fluorescence images (Fig. S11) of the B16F10 cells incubated with the hybrid nanogels further demonstrates that the hybrid nanogels can overcome cellular barriers to enter into the intracellular region. The hybrid nanogels are located in the cytoplasm and appear not to exist in the karyons. As the complexity of molecular interactions governing endocytosis are revealed, the mechanisms of endocytosis should be viewed in a broader context than simple vesicular trafficking.

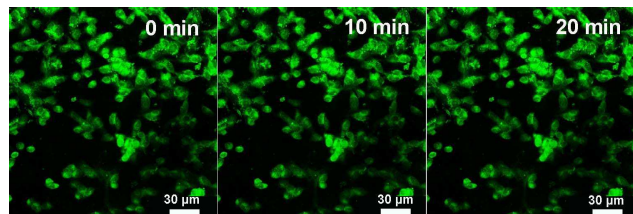


Fig. 7. Laser scanning confocal microscopy images of B16F10 cells incubated with the as-obtained hybrid nanogels under different excitation time. Excitation wavelength = 405 nm.

3.7. Cell viability evaluation of in vitro chemo, photothermal, and chemo-photothermal treatments

For future biological applications, materials should be non- or low-cytotoxic. As shown in Fig. 7, no signs of morphological damage to the cells were observed upon treatment with the free nanogels, thereby demonstrating their minimal cytotoxicity. Meanwhile, in vitro cytotoxic activity of the as-synthesized free nanogels and curcumin-loaded nanogels without/with 1.5 W/cm² NIR for 5 min was tested by means of an MTT test against B16F10 cells, as shown in Fig. 8. The results (Fig. 8a, black squares) indicate that the drug-free hybrid nanogels have negligible cytotoxicity against B16F10 cells after 24 h incubation in concentrations up to 200 μg/mL. However, the cell viability (Fig. 8a, white squares) of the drug-free hybrid nanogels under the radiation of NIR for 5 mins reduced by ~20% at the same concentrations, which indicates their photothermal therapeutic ability. In addition, compared with drug-free hybrid nanogels, the cell viability (Fig. 8a, black dot) decreased by about 25 % for the curcumin-loaded hybrid nanogels at the same concentrations. Furthermore, when the NIR light for 5 min was introduced together with the curcumin-loaded hybrid nanogels, the cell viability (Fig. 8a, white dot) decreased by ~50 %. The enhanced cytotoxicity of the curcumin-loaded hybrid nanogels with NIR radiation should be attributed to the synergistic effect of photothermal/thermo-therapy (Fig. S12).⁷¹ Fig. 8b shows in vitro cytotoxicity of curcumin-loaded hybrid nanogels at concentrations of 100 μg/mL and 200 μg/mL without/with NIR radiation under different incubated time with cells. Data shows that the viability of cells incubated with curcumin-loaded hybrid nanogels at a concentration of 200 μg/mL is always lower than that incubated with the curcumin-loaded hybrid nanogels at a concentration of 100 μg/mL when the incubated time is the same. Meanwhile, the cytotoxicity of curcumin-loaded hybrid nanogels will further increase when the 5 min NIR radiation was introduced. All above results indicate that the multifunctional core-shell nanogels based on fluorescent carbon shell and magnetic core nanoparticles can be used as promising drug carrier for combined photothermo/chemo-therapy.

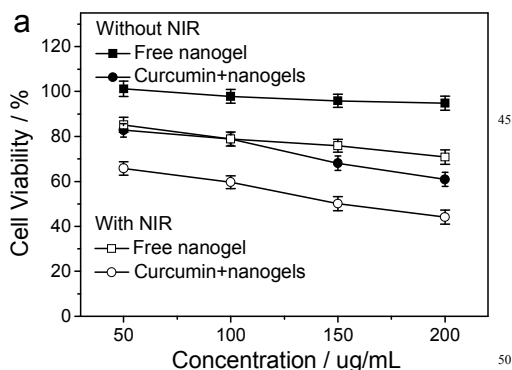
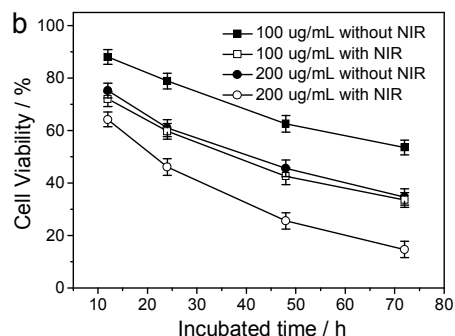


Fig.



8. (a) In vitro cytotoxicity of hybrid nanogels and curcumin loaded hybrid nanogels without/with 1.5 W/cm² NIR for 5 min, respectively; (b) In vitro cytotoxicity of curcumin-loaded hybrid nanogels at two different concentrations under different incubated time with cells without/with 1.5 W/cm² NIR for 5 min.

4. Conclusions

In summary, multifunctional core-shell hybrid nanogels have been successfully synthesized through the precipitation polymerization coating of the BFNPs with a thermo-responsive poly(NIPAM-AAm)-based hydrogel as shell. The BFNPs-functionalized hybrid nanogels exhibit high colloidal stability, excellent photoluminescent and superparamagnetic properties. The multifunctional hybrid nanogels can overcome cellular barriers to enter the intracellular region and be used as optical imaging agent to light up the B16F10 cells. The outer poly(NIPAM-AAm)-based gel shell cannot only modify the physicochemical environment of the BFNPs core to manipulate the fluorescence intensity for the sensor of the environmental temperature variation, but also provide a high loading capacity for a targeted anticancer drug. In addition, the drug release rate can be efficiently controlled by changing the temperature of local environmental media to realize reversible thermo-responsive volume phase transition or by exogenous stimuli with NIR light or alternating magnetic field. Furthermore, while the drug-free hybrid nanogels are nontoxic to cells, the curcumin-loaded hybrid nanogels exhibit potent cytotoxicity against B16F10 cells, indicating that the hybrid nanogels can be used as efficient drug carrier for treatment of tumor cells. The demonstrated BFNPs-functionalized hybrid nanogels with excellent photoluminescent and superparamagnetic properties provide a new idea for the synthesis of multifunctional fluorescent hybrid nanogels.

Acknowledgements

We gratefully acknowledge the financial support from American Diabetes Association (Basic Science Award 1-12-BS-243) and the PSC-CUNY Research Award (66076-00 44).

Notes and references

Department of Chemistry, The College of Staten Island, and The Graduate Center, The City University of New York, Staten Island, NY 10314 USA. E-mail address: shuqin.zhou@csi.cuny.edu; Tel.: +1 718 982 3897; Fax: +1 718 982 3910.

† Electronic Supplementary Information (ESI) available: Figure S1- Figure S12. See DOI: 10.1039/b000000x/

References

95 I A. Döring, W. Birbaum and D. Kuckling, *Chem. Soc. Rev.*, 2013, **42**, 7391.

- 2 M. Motornov, Y. Roiter, I. Tokarev and S. Minko, *Prog. Polym. Sci.*, 2010, **35**, 174.
- 3 M. H. Smith and L. A. Lyon, *Acc. Chem. Res.*, 2012, **45**, 985.
- 4 T. Y. Liu, S. H. Hu, D. M. Liu, S. Y. Chen and I. W. Chen, *Nano Today*, 2009, **4**, 52.
- 5 W. Wu, J. Shen, P. Banerjee and S. Zhou, *Adv. Funct. Mater.*, 2011, **21**, 2830.
- 6 A. Riedinger, M. P. Leal, S. R. Deka, C. George, I. R. Franchini, A. Falqui, R. Cingolani and T. Pellegrino, *Nano Lett.*, 2011, **11**, 3136.
- 7 M. Oishi and Y. Nagasaki, *Nanomedicine*, 2010, **5**, 451.
- 8 Z. Zhang, Y. Xu, Y. Ma, L. Qiu, Y. Wang, J. Kong and H. M. Xiong, *Angew. Chem., Int. Ed.*, 2013, **52**, 4127.
- 9 Y. Wang, G. Wu, X. Li, Y. Wang, H. Gao and J. Ma, *Biomater. Sci.*, 2013, **1**, 614.
- 10 P. Rai, S. Mallidi, X. Zheng, R. Rahmzadeh, Y. Mir, S. Elrington, A. Khurshid and T. Hasan, *Adv. Drug Deliver Rev.*, 2010, **62**, 1094.
- 11 M. H. Xiong, Y. J. Li, Y. Bao, X. Z. Yang, B. Hu and J. Wang, *Adv. Mater.*, 2012, **24**, 6175.
- 12 H. Maeda, T. Sawa and T. Konno, *J. Control. Release*, 2001, **74**, 47.
- 13 Z. M. Qian, H. Li, H. Sun and K. Ho, *Pharmacol. Rev.*, 2002, **54**, 561.
- 14 S. Stolnik, L. Illum and S. S. Davis, *Adv. Drug Deliver Rev.*, 1995, **16**, 195.
- 15 N. A. Peppas, P. Bures, W. Leobandung and H. Ichikawa, *Eur. J. Pharm. Biopharm.*, 2000, **50**, 27.
- 16 C. S. Brazel, *Pharm. Res.*, 2009, **26**, 644.
- 17 J. J. Lai, J. M. Hoffman, M. Ebara, A. S. Hoffman, C. Estournès, A. Wattiaux and P. S. Stayton, *Langmuir*, 2007, **23**, 7385.
- 18 S. F. Medeiros, A. M. Santos, H. Fessi and A. Elaissari, *Int. J. Pharm.*, 2011, **403**, 139.
- 19 W. Wu, J. Shen, Z. Gai, K. Hong, P. Banerjee and S. Zhou, *Biomaterials*, 2011, **32**, 9876.
- 20 L. Jiang, Q. Zhou, K. Mu, H. Xie, Y. Zhu, W. Zhu, Y. Zhao, H. Xu and X. Yang, *Biomaterials*, 2013, **34**, 7418.
- 21 M. P. Leal, A. Torti, A. Riedinger, R. La Fleur, D. Petti, R. Cingolani, R. Bertacco and T. Pellegrino, *ACS Nano*, 2012, **6**, 10535.
- 22 T. Y. Liu, K. H. Liu, D. M. Liu, S. Y. Chen and I. W. Chen, *Adv. Funct. Mater.*, 2009, **19**, 616.
- 23 I. Ankareddi, M. L. Hampel, M. K. Sewell, D. H. Kim and C. S. Brazel, *NSTI Nanotech.*, 2007, **2**, 431.
- 24 T. Y. Liu, S. H. Hu, T. Y. Liu, D. M. Liu and S. Y. Chen, *Langmuir*, 2006, **22**, 5974.
- 25 S. R. Deka, A. Quarta, R. Di Corato, A. Riedinger, R. Cingolani and T. Pellegrino, *Nanoscale*, 2011, **3**, 619.
- 26 P. Pradhan, J. Giri, F. Rieken, C. Koch, O. Mykhaylyk, M. Döblinger, R. Banerjee, D. Bahadur and C. Plank, *J. Control. Release*, 2010, **142**, 108.
- 27 J. Qin, I. Asempah, S. Laurent, A. Fornara, R. N. Muller and M. Muhammed, *Adv. Mater.*, 2009, **21**, 1354.
- 28 A. M. Hawkins, C. E. Bottom, Z. Liang, D. A. Puleo and J. Z. Hilt, *Adv. Healthcare Mater.*, 2012, **1**, 96.
- 29 A. Chan, R. P. Orme, R. A. Fricker and P. Roach, *Adv. Drug Delivery Rev.*, 2013, **65**, 497.
- 30 J. H. Byeon and J. W. Kim, *ACS Macro Lett.*, 2014, **3**, 369.
- 31 X. Zhang, O. Alloul, J. Zhu, Q. He, Z. Luo, H. A. Colorado, N. Haldolaarachchige, D. P. Young, T. D. Shen, S. Wei and Z. Guo, *RSC Adv.*, 2013, **3**, 9453.
- 32 J. Zhu, R. Sadu, S. Wei, D. H. Chen, N. Haldolaarachchige, Z. Luo, J. A. Gomes, D. P. Young and Z. Guo, *ECS J. Solid State Sci. Technol.*, 2012, **1**, M1–M5.
- 33 X. Zhang, O. Alloul, Q. He, J. Zhu, M. J. Verde, Y. Li, S. Wei and Z. Guo, *Polymer*, 2013, **54**, 3594.
- 34 F. F. Jöbsis vander-Vleit, *J. Biomed. Opt.*, 1999, **4**, 392.
- 35 M. Ferrari and V. Quaresima, *Neuroimage*, 2012, **63**, 921.
- 36 H. Wang, J. Shen, G. Cao, Z. Gai, K. Hong, P. R. Debata, P. Banerjee and S. Zhou, *J. Mater. Chem. B*, 2013, **1**, 6225.
- 37 M. Ma, H. Chen, Y. Chen, X. Wang, F. Chen, X. Cui and J. Shi, *Biomaterials*, 2012, **33**, 989.
- 38 M. S. Yavuz, Y. Cheng, J. Chen, C. M. Copley, Q. Zhang, M. Rycenga, J. Xie, C. Kim, K. H. Song, A. G. Schwartz, L. V. Wang and Y. Xia, *Nat. Mater.*, 2009, **8**, 935.
- 39 S. M. Lee, H. Park and K. H. Yoo, *Adv. Mater.*, 2010, **22**, 4049.
- 40 H. Liu, D. Chen, L. Li, T. Liu, L. Tan, X. Wu and F. Tan, *Angew. Chem., Int. Ed.*, 2011, **50**, 891.
- 41 A. Sánchez-Iglesias, M. Grzelczak, B. Rodríguez-González, P. Guardia-Girós, I. Pastoriza-Santos, J. Pérez-Juste, M. Prato and L. M. Liz-Marzán, *ACS Nano*, 2009, **3**, 3184.
- 42 P. G. Luo, S. Sahu, S. T. Yang, S. K. Sonkar, J. Wang, H. Wang, G. E. LeCroy, L. Cao and Y. P. Sun, *J. Mater. Chem. B*, 2013, **1**, 2116.
- 43 H. U. Lee, S. Y. Park, E. S. Park, B. Son, S. C. Lee, J. W. Lee, Y. C. Lee, K. S. Kang, M. I. Kim, H. G. Park, S. Choi, Y. S. Huh, S. Y. Lee, K. B. Lee, Y. K. Oh and J. Lee, *Sci. Rep.*, 2014, **4**, 4665.
- 44 S. Yang, X. Wang, H. Wang, F. Lu, P. Luo, L. Cao, M. J. Mezziani, J. H. Liu, Y. Liu, M. Chen, Y. Huang and Y. P. Sun, *J. Phys. Chem. C*, 2009, **113**, 18110.
- 45 K. Kawata, M. Osawa and S. Okabe, *Environ. Sci. Technol.*, 2009, **43**, 6046.
- 46 Y. Pan, S. Neuss, A. Leifert, M. Fischler, F. Wen, U. Simon, G. Schmid, W. Brandau and W. Jahnen-Dechent, *Small*, 2007, **3**, 1941.
- 47 W. M. Elshahawy, I. Watanabe and P. Kramer, *Dent. Mater.*, 2009, **25**, 1551.
- 48 M. Z. Hossain and M. G. Kleve, *Int. J. Nanomed.*, 2011, **6**, 475.
- 49 S. Dandamudi and R. B. Campbell, *Biomaterials*, 2007, **28**, 4673.
- 50 S. N. Baker and G. A. Baker, *Angew. Chem., Int. Ed.*, 2010, **49**, 6726.
- 51 H. Wang, J. Sheng, Y. Li, Z. Wei, G. Cao, Z. Gai, K. Hong, P. Banerjee and S. Zhou, *Biomater. Sci.*, 2014, **2**, 915.
- 52 H. Wang, F. Ke, A. Mararenko, Z. Wei, P. Banerjee and S. Zhou, *Nanoscale*, 2014, **6**, 7443.
- 53 H. Wang, Q. W. Chen, L. X. Sun, H. P. Qi, X. Yang, S. Zhou and J. Xiong, *Langmuir*, 2009, **25**, 7135.
- 54 S. L. Hu, K. Y. Niu, J. Sun, J. Yang, N. Q. Zhao and X. W. Du, *J. Mater. Chem.*, 2009, **19**, 484.
- 55 S. J. Yu, M. W. Kang, H. C. Chang, K. M. Chen and Y. C. Yu, *J. Am. Chem. Soc.*, 2005, **127**, 17604.
- 56 Y. R. Chang, H. Y. Lee, K. Chen, C. C. Chang, D. S. Tsai, C. C. Fu, T. S. Lim, Y. K. Tzeng, C. Y. Fang, C. C. Han, H. C. Chang and W. Fann, *Nat. Nanotechnol.*, 2008, **3**, 284.
- 57 Y. Sun, B. Zhou, Y. Lin, W. Wang, K. A. Shiral Fernando, P. Pathak, M. Mezziani, B. A. Harruff, X. Wang, H. Wang, P. G. Luo, H. Yang, M. Kose, B. Chen, L. M. Veca and S. Xie, *J. Am. Chem. Soc.*, 2006, **128**, 7756.
- 58 L. Bao, Z. L. Zhang, Z. Q. Tian, L. Zhang, C. Liu, Y. Lin, B. Qi and D. W. Pang, *Adv. Mater.*, 2011, **23**, 5801.
- 59 X. Zhai, P. Zhang, C. Liu, T. Bai, W. Li, L. Dai and W. Liu, *Chem. Commun.*, 2012, **48**, 7955.
- 60 X. Li, S. Zhang, S. A. Kulinich, Y. Liu, H. Zeng, *Sci. Rep.*, 2014, **4**, 4976; DOI: 10.1038/srep04796.
- 61 X. Wang, K. Qu, B. Xu, J. Ren and X. Qu, *Nano Res.*, 2011, **4**, 908.
- 62 R. Contreras-Cáceres, A. Sánchez-Iglesias, M. Karg, I. Pastoriza-Santos, J. Pérez-Juste, J. Pacifico, T. Hellweg, A. Fernández-Barbero and L. M. Liz-Marzán, *Adv. Mater.*, 2008, **20**, 1666.
- 63 X. Wang, L. Cao, F. Lu, M. J. Mezziani, H. Li, G. Qi, B. Zhou, B. A. Harruff, F. Kermarrec and Y. P. Sun, *Chem. Commun.*, 2009, **45**, 3774.
- 64 S. R. Wuister, C. M. Donegá and A. Meijerink, *J. Am. Chem. Soc.*, 2004, **126**, 10397.
- 65 B. B. Aggarwal and B. Sung, *Trends Pharmacol. Sci.*, 2008, **30**, 85.
- 66 B. B. Aggarwal, C. Sundaram, N. Malani and H. Ichikawa, *Adv. Exp. Med. Biol.*, 2007, **595**, 1.
- 67 S. Chang, X. Wu, Y. Li, D. Niu, Z. Ma, W. Zhao, J. Gu, W. Dong, F. Ding, W. Zhu and J. Shi, *Adv. Healthcare Mater.*, 2012, **1**, 475.
- 68 J. T. Robinson, S. M. Tabakman, Y. Liang, H. Wang, H. S. Casalongue, D. Vinh and H. Dai, *J. Am. Chem. Soc.*, 2011, **133**, 6825.
- 69 K. Yang, S. Zhang, G. Zhang, X. Sun, S. Lee and Z. Liu, *Nano Lett.*, 2010, **10**, 3318.
- 70 S. D. Conner and S. L. Schmlid, *Nature*, 2003, **422**, 37.
- 71 W. T. Wu, J. Shen, P. Banerjee and S. Q. Zhou, *Biomaterials*, 2011, **32**, 598.